

International Conference on Space Optics—ICSO 2022

Dubrovnik, Croatia

3–7 October 2022

Edited by Kyriaki Minoglou, Nikos Karafolas, and Bruno Cugny,



The X-ray testing of Einstein Probe Wide-field X-ray Telescope Qualification Model at PANTER



The X-ray testing of Einstein Probe Wide-field X-ray Telescope Qualification Model at PANTER

Surangkha Rukdee^a, Vadim Burwitz^a, Gisela Hartner^a, Thomas Müller^a, Thomas Schmidt^a, Andreas Langmeier^a, Peter Friedrich^a, Charlotte Feldman^b, Paul O'Brien^b, Richard Willingale^b, Chen Zhang^{c,d}, Zhixing Ling^{c,d}, and Weimin Yuan^{c,d}

^aMPI for Extraterrestrial Physics, Giessenbachstrasse 1, 85748 Garching, Germany

^bUniversity of Leicester, University Road, Leicester, LE1 7RH, UK

^cNational Astronomical Observatories, Chinese Academy of Sciences, 20A Datun Road, Chaoyang District, Beijing, China

^dSchool of Astronomy and Space Science, University of Chinese Academy of Sciences, Beijing, China

ABSTRACT

Wide-field X-ray Telescope (WXT) is a survey instrument of Einstein Probe, a small-class mission dedicated to time-domain high-energy astrophysics to discover transients and monitor variable objects in the 0.5–4.0 keV X-rays. We aim to characterize the performance of Qualification Model (QM) of the Einstein Probe Wide-field X-ray Telescope (WXT) – to determine the half-energy width (HEW) on-axis and off-axis, and the energy-dependent efficiency. The WXT optics assembly, consisting of 36 Micro Pore Optic (MPO) chips divided into four 3x3 MPO sectors which focus onto separate detectors. The full characterization consists of the focus searches, focal plane mapping and effective area measurements at different energies: C-K, Cu-L, Ti-K, very low Energy band continuum (vLEbc), and low Energy band continuum (lEbc). Measurements were made using the TRoPIC detector (pnCCD), a prototype of the eROSITA camera. The focal plane mapping results show an expected slight degradation towards the furthest off-axis angles as well the known alignment imperfections of some of the MPOs. The effective area results of the Energy band continuum match well with the theoretical model. This work describes the X-ray testing of the WXT QM3 Qualification Model at the PANTER X-ray test facility of the Max-Planck Institute for extraterrestrial Physics in Germany. The test setup, measurements and results are presented.

Keywords: Lobster Eyes, X-ray, Calibration, Instrumentation, Micro Pore Optics

1. INTRODUCTION

The Einstein Probe (EP)¹ is a dedicated mission to time-domain high-energy astrophysics led the Chinese Academy of Sciences (CAS) due to launch in 2023. The primary goals of the mission are to discover high-energy transients, to monitor variable objects and to search for X-ray sources associated with gravitational-wave events. The instruments on board consist of 1) the Wide-Field X-ray Telescope (WXT)² providing wide field of view observations within the energy range of 0.5-4 keV³ and 2) the Follow-Up X-ray Telescope (FXT)⁴ for the energy range 0.3-10 keV high resolution follow-up observations.

The WXT is a lobster eye type X-ray telescope consisting of 12 identical modules of 6x6 micro pore optics (MPOs). Each MPO is 2.5 mm thick and made from lead glass, with iridium coating and an aluminium film on the front. This optic has a focal length of 375 mm and a 3,600 square degrees field of view with a goal of 5 arcmin resolution. The focus point of each optic sector is aligned to its corresponding CMOS detector. The MPOs are individually aligned on the frame using screws at the rear of the frame and held in place with epoxy. Each MPO is held on the frame using an MPO enforcement pad and then secured using GD-414c silicone glue with small areas close to the MPOs filled with 703 silicone glue.⁵ The main requirement for testing the qualification model (QM) of this optic is to understand the effective area of the module and the linearity of the off-axis response.

Further author information: (Send correspondence to S.R.)
S.R.: E-mail: suri@mpe.mpg.de

2. SETUP & ALIGNMENT

The coordinate system for the optics when mounted in the chamber is diagrammatically portrayed in Figure 1. An aperture of 5.5 mm was mounted 1.5 mm from the X-ray source. For a source-detector distance of 130 m, this aperture creates a beam with a diameter of approx. 440 mm at the optic. A movable mask is mounted in front of the optic. The mask has 130×130 mm size to cover the mount frame so that the reflections from the mount frame/housing do not contaminate the measurement. With the nominal focal length of 375 mm, the derived distance, for the PANTER facility, from the Küche side of the optic to the detector chip becomes 309.5 mm.

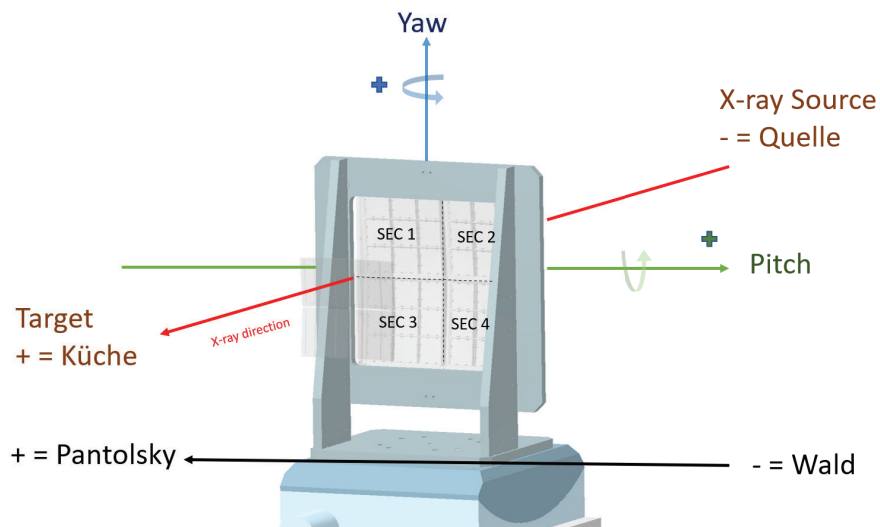


Figure 1. The PANTER coordinate system. The EP-WXT is mounted on the manipulator. The different sectors are labeled.

2.1 Alignment

To make the alignment of the X-ray image on the detector easier, alignment using a visible laser is carried out before the chamber is closed and put under vacuum. The laser is mounted in the same position as the X-ray source and the beam travels down the same beam-line to the optics. A metal cross-bar, made for the QM MOP campaign, was re-used as the central section of the MOP interface plate, to assist with the alignment of the frame in the chamber. The interface plate was mounted in the chamber and translated in Wald-Pantolsky until the alignment laser was visible on the cross-bar. Once the interface plate was aligned to the laser, the MOP was mounted to the interface plate. The laser position is visible on the MOP in Figure 2 at the center of the MOP. This was noted as the 'laser alignment' position of the MOP. Later this position was recorded under X-ray beam as a reference position. The corresponding image is shown in Figure 3 on the right side of the image where the left side is the simulated result of the intersection of the four sectors in the middle of the mirror module.

3. MEASUREMENT METHODS

3.1 Focus search

A focus search was made at Cu-L, Ti-K, C-K, very low Energy band continuum (vLEbc), and low Energy band continuum (LEbc). The optic was moved in Quelle-Küche by ± 12 mm in 4 mm steps around the nominal focus position. The count rate was recorded for each position. For this campaign, the FWHM was used as the focus search metric, and was calculated by fitting a simple Gaussian function to the profile curves in x- and y-direction of the PSF image. The minimum of the best fit ($\text{FWHM} (x+y)/2$ and relative position) was taken as the best focus position. The analysis has been done independently by the PANTER team and the by University of Leicester (UoL) team. The UoL focus position was used as the 'best focus' position for the campaign.

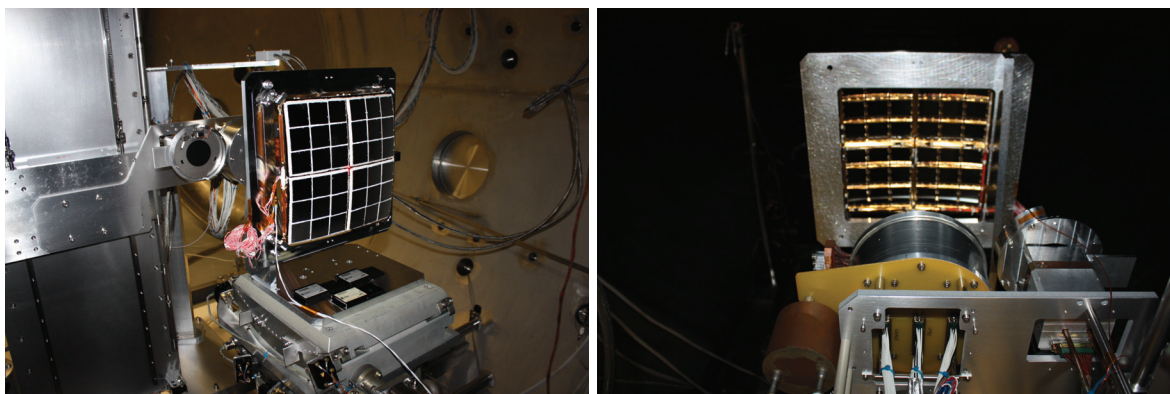


Figure 2. The WXT installed inside the PANTER chamber. (Left) The MPO mounted in the chamber, with the alignment laser centred on the MPO and the TRoPIC camera visible in the background (photo taken facing Pantolsky-Küche. (Right) The back side of the MPO inside the chamber.

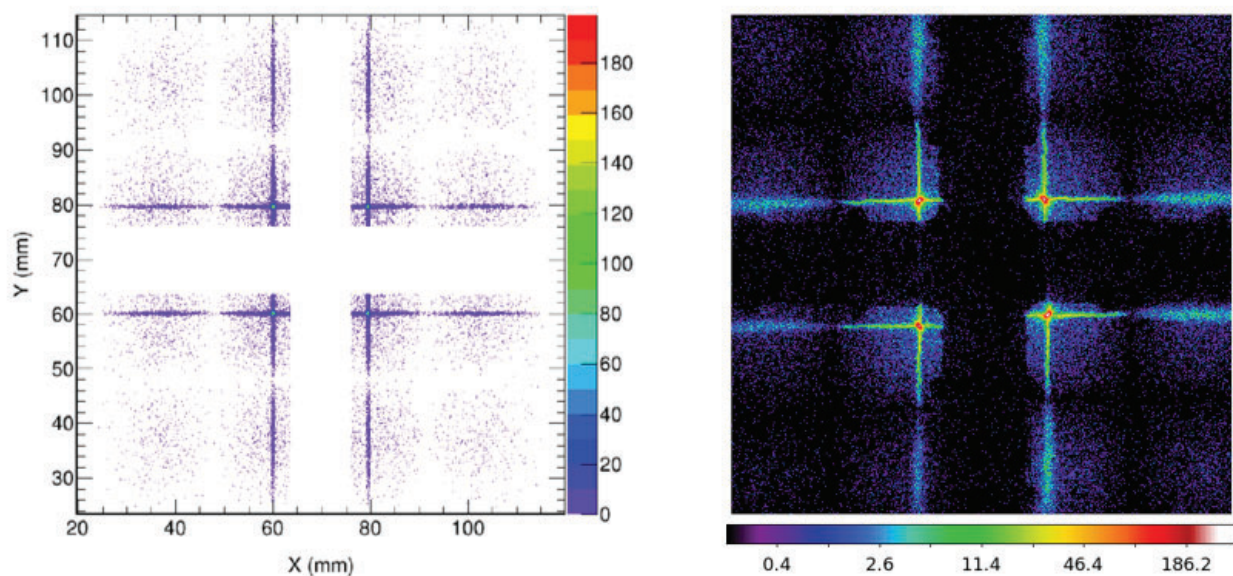


Figure 3. The first image of alignment under X-ray (right) compare to the simulated result (left)⁵

3.2 On-Axis Extended Mosaic PSF

An extended PSF image was made at energies: Cu-L, Ti-K and vEbc to characterise the extended arms of the on-axis PSF. This is a 3×3 TRoPIC scan of the on-axis in focus PSF. The nine images are then combined into one ‘mosaic’ image, to show the full PSF. The image size is $3 \times 3 \times 18.6 \times 18.6$ mm (approx. 3 TRoPIC FOVs, with a $600 \mu\text{m}$ overlap corresponds to $18.6 \times 18.6 \text{ mm}^2$ ($19.2 \times 19.2 \text{ mm}^2$ is the whole TRoPIC size).

3.3 Focal plane mapping

Focal plane mapping was carried out at each energy. The optic was moved into the best focus position and tilted in yaw by ± 150 arcmin in 50 arcmin steps, whilst remaining in best pitch position. The detector was translated in Wald-Pantolsky to follow the PSF. The pitch was then altered by ± 150 arcmin in 50 arcmin steps, with the optic in best yaw position. Once these two sets of measurements had been made, the first diagonal scan was made. The pitch and yaw were both altered by ± 150 arcmin in 50 arcmin steps (e.g., -150 arcmin pitch and -150 arcmin yaw). The second diagonal scan of alternating pitch and yaw positions (i.e., +150 arcmin pitch and -150 arcmin yaw) was made. These four scans allowed a map of the focal plane to be made. Each position exposure

was 300 seconds. These four scans allowed a ‘map’ of the focal plane to be created. For the key energies (Cu-L, C-K, and Ti-K) the full range was used.

3.4 Effective Area

The effective area A_{eff} was calculated using Equation 1, where C_{optic} is the count rate from the optic, C_{FF} is the flat field count rate, A_{det} is the collecting area of the detector (3.542 cm^2), and G is the geometrical correction for the divergent X-ray beam.

$$A_{\text{eff}} = \frac{C_{\text{optic}}}{C_{\text{FF}}} \times A_{\text{det}} \times G \quad (1)$$

The geometrical correction, G , is calculated using Equation 2, where the distance between the source and the optic is $d_{\text{source-optic}}$. The effective area is measured at the image distance d_{image} . The value for G for this campaign is 0.994.

$$G = \left(\frac{d_{\text{source-optic}}}{d_{\text{source-optic}} + d_{\text{image}}} \right)^2 \quad (2)$$

The 1σ relative statistical error is calculated for each exposure, using the number of counts in the region of interest on the detector. This error is propagated through the above calculation to give a 1σ error on the effective area value of each exposure.

3.5 Flat field

A flat field exposure was taken before and after each measurement set. The flat field exposures serve as a reference for the X-ray beam, as the collecting area of detector is well defined; the region of interest of TRoPIC is 3.542 cm^2 . During a flat field measurement, the optic is removed from the X-ray beam, and TRoPIC remains in the on-axis, in-focus position. The use of two flat field exposures accounts for possible beam variations over the measurement period. Multiple flat field exposures allow analysis of the beam stability over hours. The optic was moved out by 300 mm to Pantolsky in this campaign. Each flat field exposure was 900 seconds.

During the flat field and effective area measurements, the beam stability was also monitored. This provides an overview of how much the count rate of the X-ray beam at that energy fluctuated over a specific measurement period.

4. RESULTS

4.1 Focus search

A focus search of the full optic was carried out for the following energies: Cu-L and Ti-K. The analysis of the focus search were carried out independently from the PANTER team and the UoL team – see Table 1. It was decided to use the best focus of the UoL for this campaign. The off-axis focus search was done at sector 2 at various combinations: off-axis $\pm 2.5^\circ$ yaw, off-axis $\pm 2.5^\circ$ pitch, off-axis -2.5° pitch and -2.5° yaw, off-axis $+2.5^\circ$ and $+2.5^\circ$ yaw. The PSF images are fitted with a 2D Gaussian for the FWHM. The focus search of each sector, with the calculated FWHM, is plotted against the corresponding axis position in Figure 4. The focus axis DETQK = 26416 steps corresponds to focal length of 375 mm at infinity. This includes a 9.5 mm shift due to the rotation of the optic by 5.4° in pitch and yaw to each sector with respect to 0° alignment of complete optic.

4.2 On-Axis Extended Mosaic PSF

For each of the four sectors, a 3×3 scan was made to characterise the PSF at Cu-L (Figure 5) in best pitch and yaw position and in best focus position. The additional mosaic PSF images were carried out for sector 1 and 2 at Ti-K and vIEbc as shown in Figure 6 and 7.

Table 1. Summary of the focus search result and analysis at Cu-L

Sector	focus _{PANTER} [steps]	focus _{UoL} [steps]	Δf [steps]	Δf [mm]	FWHM(x/y) [arcmin]	f _{PANTER} [mm]	f _{inf} [mm]
1	26256	26624	368	0.46	4.4	373.8	375
2	24359	24358	-1	0.00	4.7	371.4	372
3	22543	22351	-192	-0.24	3.8	369.2	372
4	22351	23099	1479	1.85	3.4	368.0	369

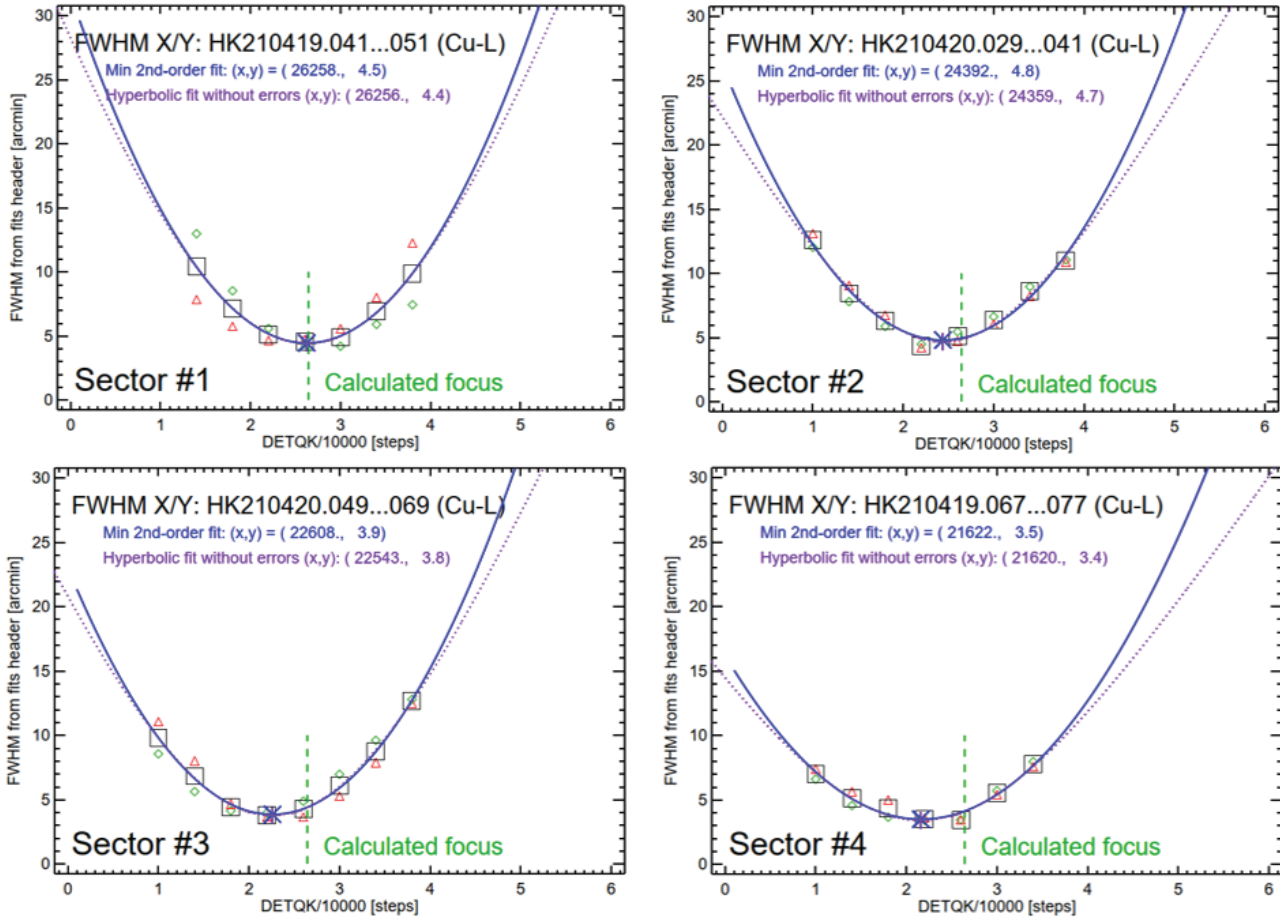


Figure 4. The focus search at Cu-L (PANTER analysis) for all sectors, with the calculated FWHM plotted against the corresponding axis position. The blue cross indicates the fitted best focus position. The green diamonds are the FWHM in x and the red triangles are the ones in y, from a simple Gaussian fit.

4.3 Focal Plane Mapping

Setting different pitch and yaw combination, the PSFs are mapped out on the focal plane both on axis and off-axis position. The scans were carried out in horizontal, vertical and diagonal directions from -150 arcmin to +150 arcmin as shown in Figure 8 at Cu-L. The missing positions from the bottom of sector 3 and 4 are due to the setup limitation. The focal plane mapping was also carried out at two additional energies: C-K and Ti-K in horizontal and vertical direction as shown in Figure 9.

4.4 Effective Area

The effective area measurements were carried out at very low Energy band continuum (vIEbc) and low Energy band continuum (lIEbc) for the single reflection, double reflection, and direct beam for all sectors. The results

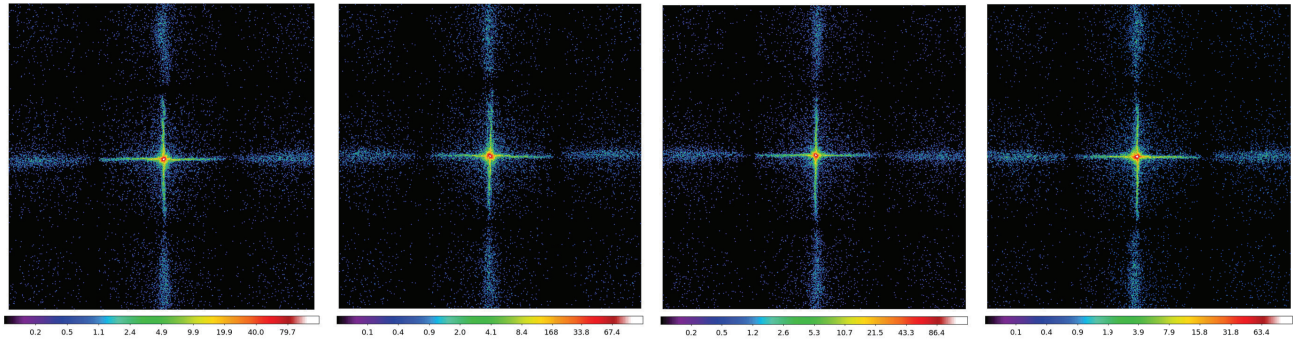


Figure 5. Compilation image of the on-axis in focus, extended (3x3) mosaic for each of the four sectors at Cu-L, from left to right are the PSF from sector 1 to 4 respectively.

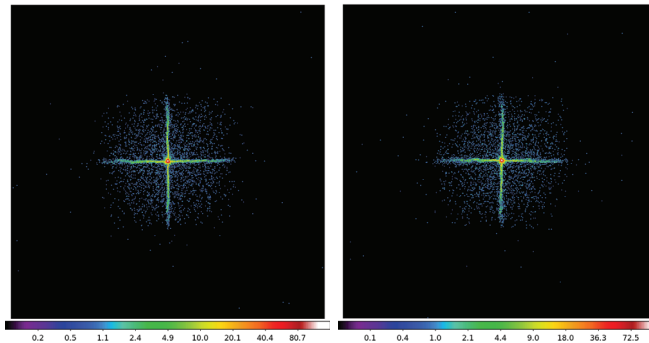


Figure 6. Compilation image of the on-axis in focus, extended (3x3) mosaic of the two sectors at Ti-K for section 1 (left) and sector 2 (right).

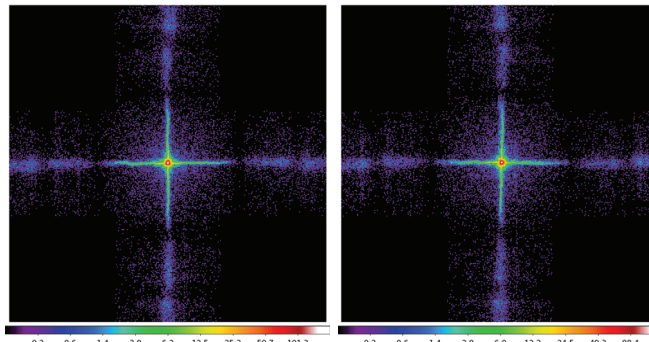


Figure 7. Compilation image of the on-axis in focus, extended (3x3) mosaic of the two sectors at vIEbc for section 1 (left) and sector 2 (right).

match well with the theoretical model from the EP team. For the vIEbc (500 - 2000 eV), the embedded lines used for the effective area calculation are O-K (525 eV) and Al-K (1490 eV). While for the lEbc (700-4000 eV), the embedded lines are Ti-L (452 eV) and W-M (1780 eV). Figure 10 shows the measurement results of the effective area at the vIEbc and lEbc overlay with the model from the EP team (Chen Model⁶) and UoL team (Dick Model). The data points from single energy measurements are also included in the plot.

5. DISCUSSION & CONCLUSION

The Einstein Probe WXT QM was tested at PANTER at the energies: very low Energy band continuum (vIEbc), low Energy band continuum (lEbc) Cu-L, Ti-K, and C-K. The mirror module has undergone measurements under X-ray. Since the TRoPIC detector is set to be perpendicular to the optical axis, not at the focal plane of each

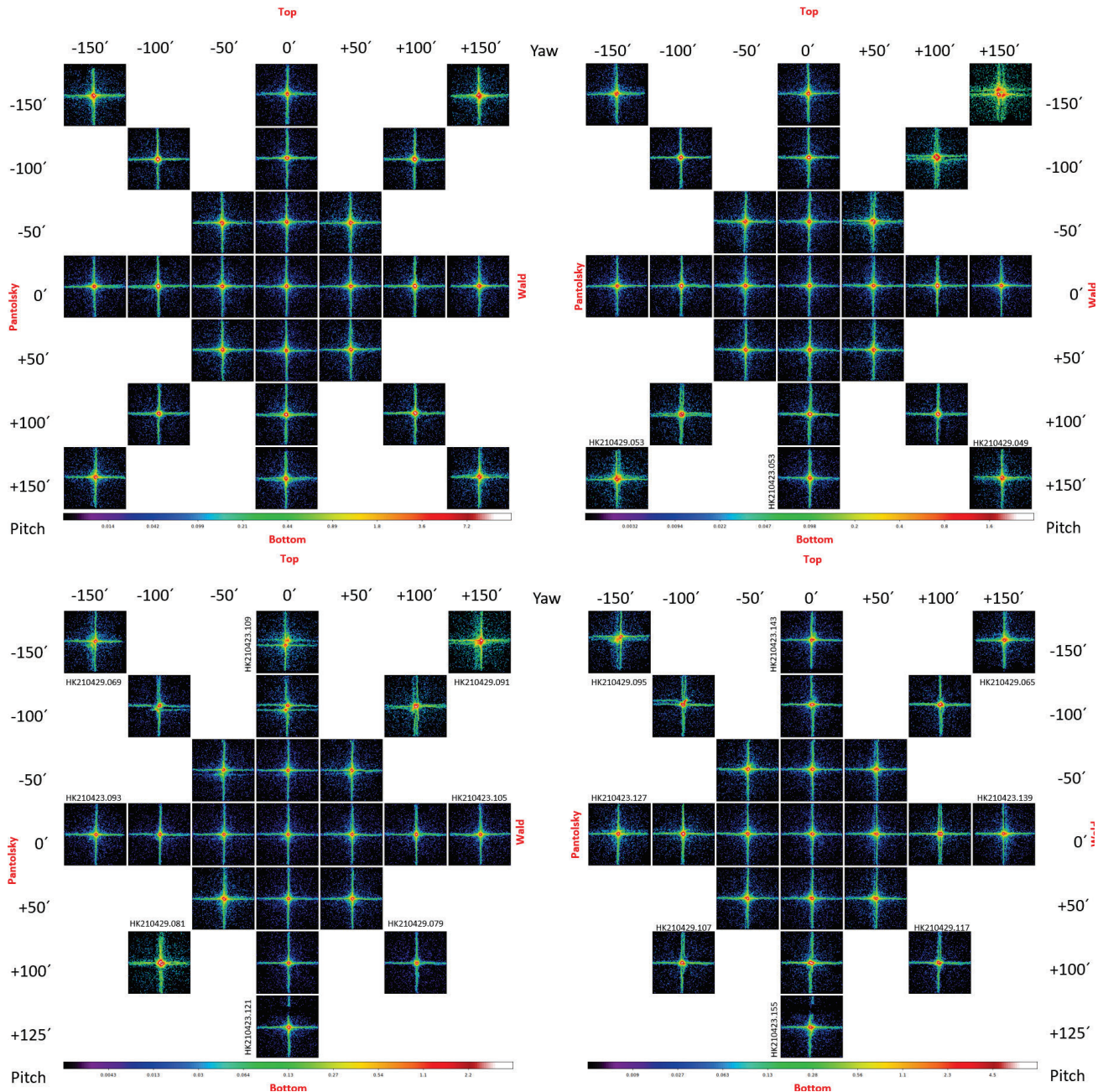


Figure 8. Compilation of PSF exposures for the focal plane mapping at all sectors: sector 1 (top left), sector 2 (top right), sector 3 (bottom left), sector 4 (bottom right) in horizontal, vertical and diagonal direction Cu-L.

sector, additional movement was required for the optic and detector to align each sector. The mirror sector was rotated by range $\pm 5.4^\circ$ in pitch and yaw with respect to the optical axis. The detector was translated in Pantolsky-Wald or Up-Down direction by 71 mm for the measurement. As a result, this introduced an additional shift of 9.5 mm along the optical axis. During the alignment under X-ray, we have noticed a slight plate misalignment at the lower right corner (sector 4) of the Figure 3 that was not well aligned with the other sectors in comparison to the simulation. However after the focus searches for all sectors, the average FWHM for all sectors was ~ 4.1 arcmin from the PANTER analysis. We have analysed the PANTER best focus with independent analysis to those of UoL on the same dataset. The best focus position for all but one sector (4) differed by less

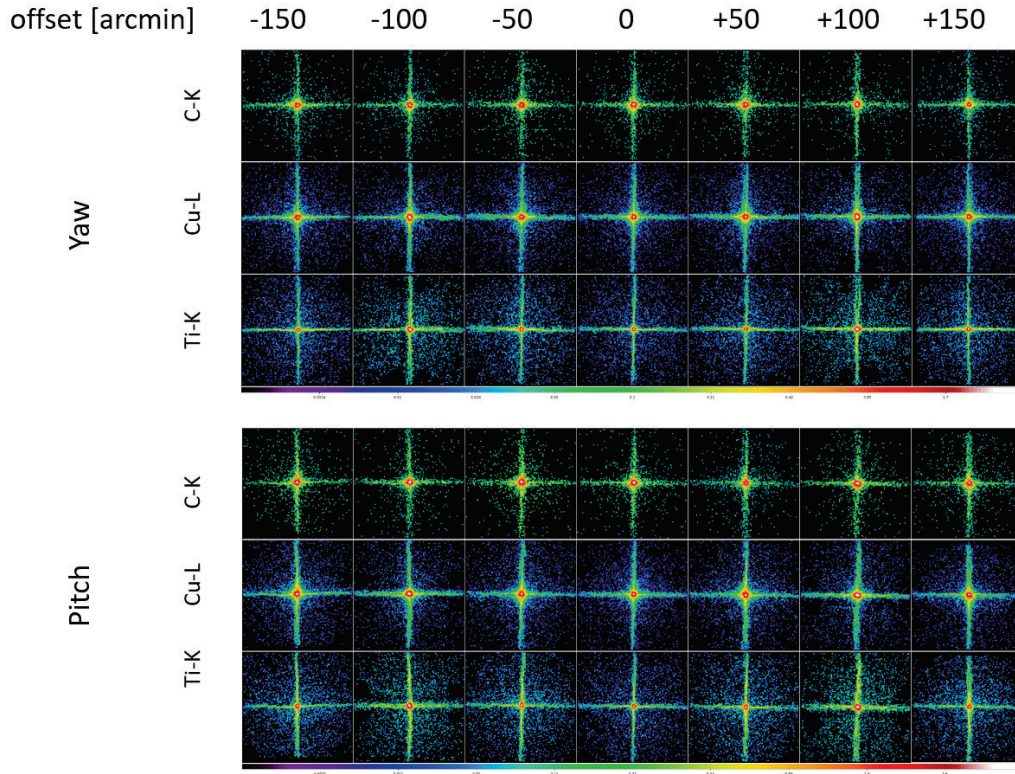


Figure 9. Compilation of PSF exposures for the focal plane mapping at sector 2 in horizontal (yaw), vertical (pitch) direction at C-K, Cu-L and Ti-K for the off-axis angle from -150 arcmin to 150 arcmin

than 0.5 mm. Sector 4 was measured to have the shortest focal length among all the sectors.

After the focal length of each sector was measured, the on-axis extended mosaic PSF was characterized. The PSF at different energies confirms that the mirrors are more sensitive (collect more X-ray photons) towards the vIEbc and Cu-L – see results in Figure 5 and 7, compare to ones taken at Ti-K in Figure 6.

A ‘map’ of the focal plane of the MOP depending on the off-axis angle was created at C-K, Ti-K and Cu-L. The resulting PSFs in their corresponding positions are displayed in a single image for each energy. The full mapping of all sectors was carried out at Cu-L including the off-axis angle ranging ± 150 arcmin shown in Figure 9. Our results shows that sector 1 has the best alignment among all the MPO chips within that sector. Sector 2 and 4 has slight separation of the single reflection, from mis-alignment of the MPOs, at the far end (± 150 arcmin) of the off-axis focal plane. Sector 3 shows a similar effect especially at the off-axis angle -50 to -150 arcmin. The characterization of the mapping only the horizontal (yaw), and vertical (pitch) at different energies shows an effect of X-ray scattering towards the higher energy. It creates ‘halo’ around the double reflection spot, clearly shown in the images taken at Ti-K. This could be caused by the micro roughness on the mirror surface.

Lastly, the effective area measurement of vIEbc and lEbc combination for all sectors agrees well with the theoretical model – see Figure 10. The number is also proportional to the quality of the alignment within each sector.

The development of the WXT mirror module has currently gone to the flight model (FM) phase. PANTER is expecting the next characterization of a WXT FM optic in Fall 2022.

ACKNOWLEDGMENTS

We acknowledge contributions from the WXT consortium and the Einstein Probe team from CAS, NAOC and the University of Leicester. Part of the work performed at PANTER has been supported by the European Union

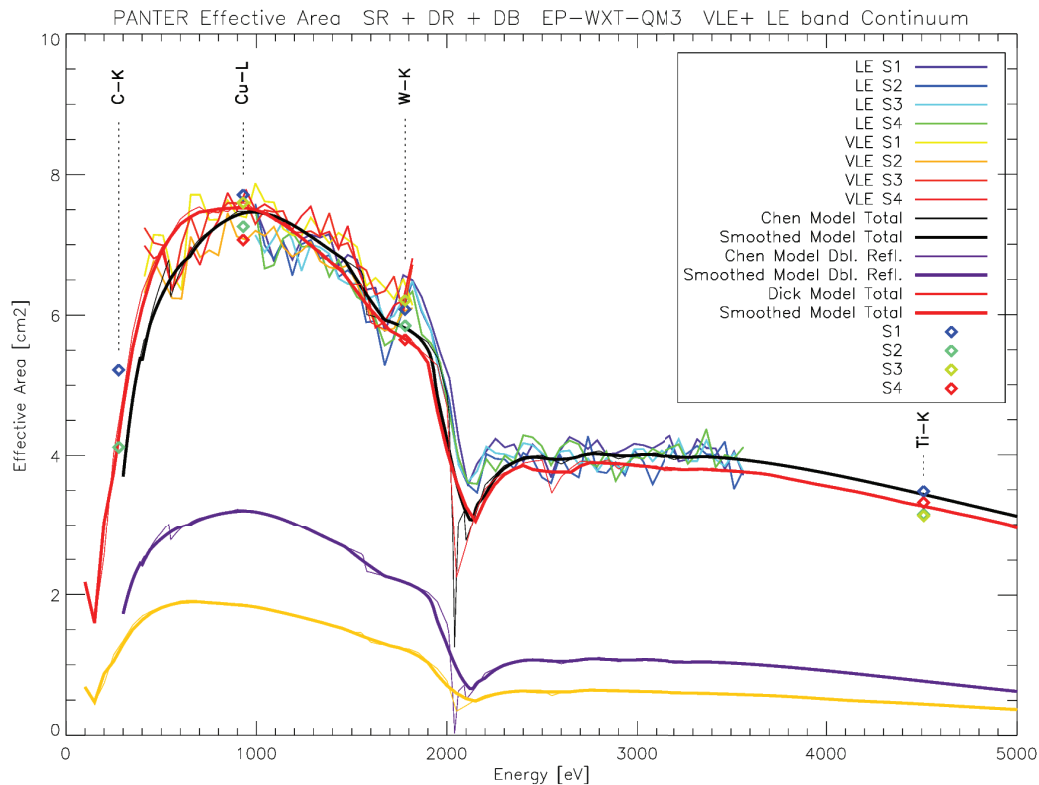


Figure 10. The effective area of single reflection, double reflection, and direct beam at vLEbc (VLE) and lEbc(LE) for all 4 sectors (S1, S2, S3, S4) in comparison with different models

Horizon 2020 Programme under the AHEAD2020 project (grant agreement n. 871158).

REFERENCES

- [1] Yuan, W., Zhang, C., Feng, H., Zhang, S. N., Ling, Z. X., Zhao, D., Deng, J., Qiu, Y., Osborne, J. P., O'Brien, P., Willingale, R., Lapington, J., Fraser, G. W., and the Einstein Probe team, "Einstein Probe - a small mission to monitor and explore the dynamic X-ray Universe," *arXiv e-prints*, arXiv:1506.07735 (June 2015).
- [2] Yuan, W., Zhang, C., Ling, Z., Zhao, D., Wang, W., Chen, Y., Lu, F., Zhang, S.-N., and Cui, W., "Einstein Probe: a lobster-eye telescope for monitoring the x-ray sky," in [*Space Telescopes and Instrumentation 2018: Ultraviolet to Gamma Ray*], den Herder, J.-W. A., Nikzad, S., and Nakazawa, K., eds., *Society of Photo-Optical Instrumentation Engineers (SPIE) Conference Series* **10699**, 1069925 (July 2018).
- [3] Feldman, C., O'Brien, P., Willingale, R., Zhang, C., Ling, Z., Yuan, W., Jia, Z., Jin, G., Li, L., Xu, Z., Zhang, Z., Lerman, H., Hutchinson, I., McHugh, M., and Lodge, A., "Testing of the WXT optics at the University of Leicester," in [*Society of Photo-Optical Instrumentation Engineers (SPIE) Conference Series*], *Society of Photo-Optical Instrumentation Engineers (SPIE) Conference Series* **11444**, 114447R (Dec. 2020).
- [4] Chen, Y., Cui, W., Han, D., Wang, J., Yang, Y., Wang, Y., Li, W., Ma, J., Xu, Y., Lu, F., Chen, H., Tang, Q., Yuan, W., Friedrich, P., Meidinger, N., Keil, I., Burwitz, V., Eder, J., Hartmann, K., Nandra, K., Keereman, A., Santovincenzo, A., Vernani, D., Bianucci, G., Valsecchi, G., Wang, B., Wang, L., Wang, D., Li, D., Sheng, L., Qiang, P., Shi, R., Chao, X., Song, Z., Zhang, Z., Huo, J., Wang, H., Cong, M., Yang, X., Hou, D., Zhao, X., Zhao, Z., Chen, T., Li, M., Zhang, T., Luo, L., Xu, J., Li, G., Zhang, Q., Bi, X., Zhu, Y., Yu, N., Chen, C., Lv, Z., Lu, B., and Zhang, J., "Status of the follow-up x-ray telescope onboard the Einstein Probe satellite," in [*Society of Photo-Optical Instrumentation Engineers (SPIE) Conference Series*], *Society of Photo-Optical Instrumentation Engineers (SPIE) Conference Series* **11444**, 114445B (Dec. 2020).

- [5] Feldman, C., “Einstein probe qm module tests at panter (tn18 for wp 1.4),” techreport Issue 1 Rev:2, University of Leicester (2021).
- [6] Zhao, D., Zhang, C., Yuan, W., Zhang, S., Willingale, R., and Ling, Z., “Geant4 simulations of a wide-angle x-ray focusing telescope,” *Experimental Astronomy* **43**, 267–283 (2017).